An Experimental Study of Mini-Tabs for Aerodynamic Load Control

D. J. Heathcote[1], I. Gursul[2], D. J. Cleaver[3]
Department of Mechanical Engineering, University of Bath, BA2 7AY, UK

Aircraft and wind turbines are exposed to increased loads during gusts and turbulence, necessitating a stronger and stiffer structure. The field of aerodynamic load control aims to reduce this need, mitigating the extreme loads at the fluid structure interface. Force, Particle Image Velocimetry and pressure measurements were conducted on a NACA0012 airfoil equipped with mini-tabs, small span-wise tabs that were to the airfoil's upper surface, at a Reynolds number of 6.61 x 10^5. Mini-tabs of height h/c = 0.02 and 0.04 were employed across a range of chord-wise locations to investigate the effects of mini-tab height and chord-wise position. Overall, the mini-tab was found to have a lift reducing effect which increased with height. It was found that the effect of the chord-wise location was highly dependent on the angle of attack. Placement close to the trailing edge induced a large effect at zero degrees. Peak suction over the lower surface increased resulting in a reduction of ΔC_L = -0.48. Approaching stall, effectiveness decreased as the mini-tab became immersed in the separated flow. Placement at x_f/c = 0.60 produced an almost constant lift reduction between α = 0° and 5° of $\Delta C_L \approx$ -0.60, with a gradual reduction to stall. A mini-tab positioned close to the leading edge (x_f/c = 0.08) was found to separate the flow effectively at low incidences but with no noticeable change in lift observed. It was found that the flow separation produced by the mini-tab effectively eliminated the suction peak on the upper surface. However, placement close to the leading edge has increasing effectiveness towards stall, as the shear layer induced by the separation was displaced further from airfoil surface. Peak lift reduction at stall was found to be $\Delta C_L \approx$ -0.67. The optimum chord-wise location for peak lift reduction is dependent on the airfoil angle of attack: the position of the mini-tab for maximum lift reduction moves towards the leading edge as the angle of attack increases.

Nomenclature

α	=	angle of attack
b	=	span
c	=	airfoil chord length
C_D	=	time-averaged drag coefficient, $D/(0.5\rho U_\infty^2 bc)$
C_L	=	time-averaged lift coefficient, $L/(0.5\rho U_\infty^2 bc)$
C_P	=	pressure coefficient, $(p - p_\infty)/(0.5\rho U_\infty^2)$
$C_{P,min}$	=	minimum pressure coefficient
ΔC_L	=	change in lift coefficient from baseline configuration
h	=	mini-tab height
n	=	exponent for theoretical relationship
Re	=	Reynolds number, $\rho U_\infty c/\mu$
p	=	surface static pressure
U_∞	=	free-stream velocity
p_∞	=	free-stream static pressure
ρ	=	fluid density
q	=	parameter for theoretical relationship

[1] Postgraduate Student, Department of Mechanical Engineering. Student Member AIAA.
[2] Professor, Department of Mechanical Engineering. Associate Fellow AIAA.
[3] Lecturer, Department of Mechanical Engineering. Member AIAA.

u = velocity component parallel to free-stream
v = velocity component perpendicular to free-stream
μ = dynamic viscosity
x = chord-wise location
x_f = mini-tab chord-wise location
y = position perpendicular to free-stream
z = span-wise location

I. Introduction

Aircraft and wind turbines are exposed to increased aerodynamic loads during gusts, turbulence and manoeuvres. These load cases are typically the most extreme, dictating the size of the structure and thus weight, even though they are rare occurences. Current actuation strategies, such as flaps and ailerons, aim to mitigate these loads at the fluid-structure interface however they are extremely limited in their frequency response due to their large inertia even though evidence[1,2] suggests that high frequency is key to an actuator's ability to effectively mitigate aerodynamic loads. Current and incoming legislation through ACARE Vision 2020 dictates that aircraft emissions must be reduced, applying pressure to reduce actuator and airframe structural weight in the coming years. In addition, novel flow technology will create a benefit to passenger comfort reducing injury and fatigue by reducing turbulent loads. These driving factors suggest a demand for an active flow technology with high frequency response in order to mitigate the extreme aerodynamic loads efficiently.

A variety of novel flow control strategies have been proposed through fluidic or mechanical means[3-5] in order to reduce the lift produced by the airfoil. The focus of the present study is a mechanical device termed the mini-tab. The mini-tab consists of a small tab placed perpendicular to the airfoil surface; placement close to the trailing edge for lift enhancement is termed a Gurney flap. The Gurney flap is a device which has been widely studied in respect to airfoil lift increase and also in providing an increase in downforce in a motorsports application. The Gurney flap produces a separated region characterized by a counter-rotating vortex pair behind the flap or tab, causing a displacement of the Kutta condition downstream. This was first hypothesized by Liebeck[6] and validated by others[7-10]. The displacement of the Kutta condition causes the final part of the pressure recovery to be performed off-surface and downstream of the trailing edge, in turn increasing the peak suction, $C_{P,min}$ on the upper surface. The Gurney flap deflects the flow at the trailing edge, causing a change in the effective airfoil camber. Placement on the lower, pressure surface creates a downturning of the flow increasing lift but providing a slight decrease in the stall angle. Theoretical modelling[11] has shown that the Gurney flap's ability to increase lift is proportional to the square root of the normalised height, h/c. In addition, sizing of the Gurney flap height less than the boundary layer thickness produces only a small effect on drag[12].

Positioning on the upper surface for lift reduction has been hypothesized and placement of a Gurney flap-style mini-tab device close to the trailing edge has been found to be an effective lift mitigation strategy[13,14] with a change in lift coefficient up to $\Delta C_l = -0.4$[15]. A similar cambering effect was observed for lower surface placement albeit in the opposite sense (negative cambering opposed to positive). Placement close to the trailing edge yielded a decreasing reduction towards stall. While mini-tab utilisation away from the trailing edge has yet to be fully investigated, slight upstream utilization ($x_f/c > 0.70$) yielded a smaller change in lift than placement directly at the trailing edge[16,17] at an angle of incidence of zero degrees. In addition, the work of Baker et al[18] suggests that employment away from the trailing edge at $x_f/c = 0.60$ produces a more significant reduction in lift, while placement at $x_f/c = 0.40$ produced a minimal effect at $\alpha = 0°$ with an increased effect towards stall. While the effects on flow due to placement close to the trailing edge are known, the effect of placement towards the leading edge is unknown. The more general term mini-tab is used thoughout to distinguish from the more specific placement and effect on flow that the Gurney flap describes. As such the Gurney flap becomes a sub-set of the mini-tab.

This paper presents an initial experimental survey of the mini-tab as a flow control device for lift mitigation. The study investigates static placement at a wide range of chord-wise locations, while simultaneously investigating the effect of mini-tab height and airfoil angle of attack using force measurements. The mini-tab's effect on the flow in the vicinity of the airfoil is evaluated by particle image velocimetry and surface pressure measurements, while an assessment of the effects of mini-tab utilization on unsteady force and instantaneous flow-field is provided. The results of the current study have informed a study of an active mini-tab actuator, where the mini-tab height is actively controlled to mitigate a gust load.

II. Experimental Apparatus and Procedure

A. Experimental Setup

All experiments were performed in the University of Bath large wind tunnel. The wind tunnel is of a closed loop design, with a test section of dimensions 2.13 x 1.51 x 2.70 m and an octagonal cross-section to reduce secondary flow effects. The freestream velocity of the tunnel was held at U_∞ = 20 ms^{-1} with a turbulent intensity of less than 0.5%. Fig. 1(a) illustrates the layout of the working section of the wind tunnel with the wing *in-situ*. A stepper-motor driven turntable above the tunnel allowed the angle of attack to be varied.

A NACA0012 airfoil profile was chosen due to its symmetry and the wide array of data available in the literature. A chord length, c = 0.5 m was chosen alongside a span, b = 1.5 m. The Reynolds number based on chord length was Re = 6.61 x 10^5. The boundary layer over the airfoil was transitioned to turbulence at x/c = 0.1 using a 0.3 mm diameter wire on both surfaces using methods described by Pankhurst and Holder[19]. The wire fixes the boundary layer transition at the point of maximum velocity as suggested by Barlow et al[20]. This is comparable location to that found at full-scale conditions (aircraft at cruise). The wing shown in Fig. 2 is designed such that the the test section is fully spanned by the wing with a small clearance (5 mm or 0.3% of the overall span). This design employs the wind tunnel walls as end plates negating tip effects while the small clearance avoids any physical interference with the wind tunnel walls ensuring accurate force measurements. The wing was constructed for two projects, the second concerned with jet-flap actuation. For jet-flap actuation, slots of width one millimetre are located at x/c = 0.08, 0.60, 0.75, 0.85 and 0.95 and were covered during the mini-tab experiments. As shown in Fig. 2 the initial 0.725c is constructed of a carbon fibre composite with an aluminium internal structure, providing stiffness and low weight. The remaining 0.275c consists of five removable selective laser sintered Nylon components allowing for the actuation method close to the trailing edge to be altered.

Mini-tabs of normalized height, h/c = 0.02 & 0.04 were constructed for the experiments using carbon fibre. The design of the tab was a simple "L"-shape of length 1.5 m and thickness 1.5 mm. The base of the tab was fixed to the wing using double-sided tape such that the tab itself was perpendicular to the airfoil surface. The chord-wise location of the mini-tab locations (x_f/c) was varied between the positions shown in Fig. 3 to allow for the effects of the chord-wise placement to be accurately determined.

B. Force Measurements

The airfoil was mounted from above via a two-component aluminium binocular strain gauge force balance, the design of which has been used extensively at the Univeristy of Bath[21,22]. The force balance consists of four strain gauges per component arranged in a Wheatstone bridge configuration. The voltage output was conditioned and acquired using a Data Translation DAQ and a LabVIEW programme. The balance was aligned parallel (x-axis) and perpendicular (y-axis) to the airfoil chord using a spigot. The forces were obtained simultaneously at 2 kHz for 20,000 sample cycles, with six repeat measurements completed per angle in order to ensure accuracy. With the angle of attack being controlled above the force balance, the measured forces were resolved to the flow direction to obtain the lift and drag forces using MATLAB. Calibration of the balance was performed before each set of experiments to ensure accuracy. The calibration was performed for each axis by applying known forces in the form of weights to the balance and measuring the voltage output to obtain a linear force-voltage calibration constant. In order to minimize uncertainty in the measurement, a minimum of 30 discrete data points between -150 N and 150 N for the y-axis and 10 N between 0 and 60 N for the x-axis were obtained.

Force measurements were completed for both mini-tab heights between α = -20 and 20° for all chord-wise locations in Fig. 3. Table 1 summarizes the experimental parameters used and their associated uncertainties.

Table 1: Table displaying experimental parameters and the values used along with associated experimental uncertainty.

Parameter	Range or Value Considered	Uncertainty
***h/c*, mini-tab height**	0.02 to 0.04	±0.001
***x_f/c*, chord-wise position**	0.08, 0.15, 0.30, 0.45, 0.60, 0.75, 0.85 & 0.95	±0.003
***Re*, Reynolds number**	6.61x10^5	±0.16x10^5
***α*, Angle of Attack**	-20° to 20°	±0.25°

C. Particle Image Velocimetry Measurements

Cases of interest were selected from the force measurements for further analysis using Particle Image Velocimetry (PIV) allowing the flow-field in the vicinity of the airfoil to be measured and the effects of the mini-tab to be fully investigated.

The flow was seeded using olive oil particles via a six jet TSI oil-droplet generator. The in-plane velocity of the particles was measured using a TSI 2D-PIV system comprising a double pulsed 200 mJ 15 Hz Nd:YAG laser, two four Megapixel TSI PowerView CCD cameras (2048 x 2048 pixels) and a TSI LaserPulse synchronizer. Further measurements were conducted at zero degrees incidence to include the wake region. For these measurements two eight Megapixel TSI PowerView CCD cameras (3,312 x 2488 pixels) were utilized. The configuration of the system is shown in Fig. 1. Fig. 1(a) shows the laser alignment to the airfoil profile. The measurement plane was placed beyond the mid-span at $z/b = 0.6$ due to the presence of pressure tappings at the mid-span. The plane was orientated normal to the airfoil surface.

Fig. 1(b) illustrates the camera set up from below. The dual cameras were mounted to a traverse below the wind tunnel in a "tandem" configuration with the same plane of interest. The cameras were rotated with the airfoil maintaining the airfoil field-of-view as the angle of attack was varied. The set up allowed measurements across the airfoil chord to be taken concurrently with a total field of view of 0.6 m x 0.35 m (0.8 m x 0.35 m for the near wake measurements), without the need for the camera to be repositioned. The cameras both used a Nikon 50 mm Nikkor lens at approximately 1.5 m from the plane of interest. The PIV measurements were performed only on the upper surface of the airfoil.

400 image pairs were captured for each camera and case concurrently. TSI Insight 3G software was used to determine in-plane velocity vectors via a fast Fourier transform cross-correlation between image pairs. An interrogation window size of 24 x 24 pixels (32 x 32 for measurements inclusive of the wake region) was used producing an effective spacial resolution of 0.22%c . The overlap between the cameras shown in Fig. 1(b) allowed the two vector fields to be merged using a custom MATLAB code with a weighted average used within the overlap region.

D. Pressure Measurements

Pressure measurements were completed for select cases in order to further assess the effect of mini-tab location on the pressure distribution. 40 pressure taps of diameter two millimetres placed at the mid-span of the wing were utilized for the measurements, as shown in Fig. 2(a), with 19 and 21 taps located on the upper and lower surfaces respectively. The tappings were connected to a rotary Scanivalve using 0.125" diameter tubing. The pressure was measured using Scanivalve Corp PDCR23 differential pressure transducer. The pressure transducer was calibrated separately using a Druck DPI portable pressure transducer calibrator. The tappings were measured sequentially at 1kHz for 3000 cycles with an additional settling delay of 0.5 seconds. Three repeat measurements were completed in order to ensure accuracy.

E. Assessment of Measurement Uncertainty

The uncertainty in each of the measurement techniques was quantified. Firstly, uncertainties in the force measurement apparatus and procedure were assessed and combined using the methods of Moffat[23]. An uncertainty in the force balance calibration coefficient was found to be of the order of 0.5%. Due to machining error, a tolerance of ±0.5 mm was placed on the span and chord of the airfoil, inducing an uncertainty in the area which was deemed negligible. The uncertainty in the free-stream dynamic pressure, q was quantified as 1.25%. The plane of interest for the PIV measurements was of the order 2 mm, with an alignment error of ±1 mm. An uncertainty in the measured pressure coefficient was quantified as ±0.06, by combining the deviation in the measured pressure and the uncertainty in free-stream dynamic pressure. Finally interference effects within the wind tunnel due to the model's interaction with the walls of the wind tunnel were evaluated using the methods of Pankhurst and Holder[19], however these were found to have an insignificant effect on the results.

III. Results and Discussion

This section initially discusses the force measurements covering a wide range of mini-tab chord-wise locations and two heights. Section A identifies the chord-wise locations for peak lift reduction, with a comparison to literature and theoretical modelling for a trailing edge location provided in section B. The locations further analysed using time-averaged PIV and pressure measurements in sections C and D respectively. Section E analyses the unsteady effects on the flow through introduction of the mini-tab.

A. Force Measurements

Fig. 4 presents time-averaged lift and drag coefficient data for h/c = 0.02 (a and c) and 0.04 (b and d) for all mini-tab chord-wise locations and the baseline configuration. The baseline configuration lift coefficient data is in good agreement with previous studies completed by Jacobs & Sherman[24] and Sheldahl & Klimas[25] at comparable Reynolds numbers. From the guidelines for stall behavior from Gault[26] it can be observed that the C_L behavior at stall is indicative of a trailing edge stall condition, consistent with predicted stall behavior for the Reynolds number and airfoil thickness. It can be observed that the mini-tab has the effect of reducing lift in all configurations, however the severity of the lift mitigation is dependent on angle of attack, mini-tab height and chord-wise location.

On the effect of mini-tab height, at zero degrees it can be observed that a mini-tab of h/c = 0.04 has a greater effect than one of h/c = 0.02 at the same chord-wise location. This can be clearly observed at x_f/c = 0.95, where a mini-tab of h/c = 0.02 produces a change in lift coefficient (ΔC_L) of -0.32 as opposed to -0.48 for h/c = 0.04. This greater effect with greater height is generally applicable.

The chord-wise location of the mini-tab has a profound effect on its ability to reduce lift at different angles of attack. Placement close to the trailing edge produces a large lift reduction at low angles of attack, with a reducing effect towards stall ($\alpha \approx 13°$). An increase in the gradient of the C_L - α curve can be observed with a large lift reduction noted at the negative stall angle, with a gradual decrease in effectiveness to a minimal change in lift at the positive stall angle.

Moving away from the trailing edge, lift mitigation is reduced for x_f/c = 0.85 and 0.75 mini-tab locations at low incidences in agreement with literature[17]. An increase in the gradient within the linear region can be observed, however of less severity than that for the x_f/c = 0.95 location. Lift reduction is once again reduced towards the stall angle.

Moreover, locating the mini-tab at x_f/c = 0.60 produces a more uniform lift reduction at low angles of incidence ($0° \leq \alpha \leq 5°$) with a peak lift reduction of -0.60 obtained for a mini-tab of height, h/c = 0.04. Beyond α = 5° a change in the gradient of the $C_L - \alpha$ curve is observed, with a reduction in the change in lift, ΔC_L observed towards stall. The non-linear change in gradient implies a constant effect between $0° \leq \alpha \leq 5°$ but beyond the effect reduces significantly towards stall.

Placement of the mini-tab close to the leading edge appears to induce no appreciable lift mitigation at zero degrees and for negative angles of attack where there is negligible change in C_L. However, close to and beyond stall lift reduction is more pronounced for both mini-tab heights (ΔC_L = -0.48 and -0.67 at α = 13° for h/c = 0.02 and 0.04 respectively). This is summarized in Fig. 5 which presents a clear and observable trend: the position of the mini-tab for maximum lift reduction moves towards the leading edge as the angle of attack increases. Fig. 5 suggests that there is a optimum region of sensitivity for mini-tab placement for lift reduction, represented by the blue region. In summary, at low angles of attack a location towards the trailing edge or mid-chord is preferable, whereas at high angles of attack a leading edge location is optimal.

The effect on time averaged drag coefficient due to the mini-tab placement is shown in Fig.s 4(c) and (d). It can be noted that the mini-tab has a detrimental effect on drag throughout, with a larger effect for increased mini-tab height. For mini-tabs located close the trailing edge the effect is consistent with Gurney flaps located at the trailing edge and whose size is large than the boundary layer thickness in the vicinity of the mini-tab[12]. The trends observed in lift coefficient for increasing angle of attack is reflected in the drag coefficient. Placement close to the trailing edge produces a decreasing impact on drag close to stall while conversely, placement in the vicinity of the leading edge has an increasing effect close to the stall angle. In the present study the effect of drag is not of a primary concern. In an active configuration the mini-tab will be used for short, transient events,where protection of the airframe and thus lift reduction is key.

From the force measurements three locations were selected for further analysis through PIV and pressure measurements: x_f/c = 0.08, 0.60 and 0.95. These were considered the cases of most interest due the disparity in their effect obtained both pre- and post-stall.

B. Comparison to Theoretical Change in Lift

A theoretical relationship between lift enhancement and the normalized Gurney flap height was determined by Liu & Montefort[11] using a vortex sheet with a displaced segment representing the Gurney flap. Due the symmetric nature of the NACA0012 profile, upper surface mini-tab employment in the vicinity of the trailing edge (x_f/c = 0.95) at zero degrees incidence is analogous to lower surface Gurney flap utilization at the same angle and the magnitude in the change in lift should be equal ($|\Delta C_{L0}|$). As such, a qualification of the lift reduction obtained in the current study can be completed in comparison to theory and previous studies[7,8,10,15,18,27-29] at their respective zero lift angles. Theory suggests that the the change in lift coefficient at the zero lift angle is related to the normalized Gurney flap height, h/c:

$$|\Delta C_{L0}| = q \times \left(\frac{h}{c}\right)^n$$

Where q is a parameter determined dependent on Reynolds number and airfoil profile and n is an exponent found by Liu & Montefort to be 0.5, however later work by Greenwell[30] suggests a value close to 0.7.

The comparison is shown in Fig. 6(a) for all airfoil profiles and in Fig. 6(b) for NACA0012 only. Two lines of best fit are displayed using the theory developed by Liu & Montefort, one strictly adhering to the suggested n = 0.5 value ("fixed n") and one for n as a free parameter ("free n.")

For the fixed condition, a trend between the normalized mini-tab height and the change in lift can be clearly observed. The coefficient of determination, R^2 indicates that the fit is improved when the NACA0012 profile is considered individually, improving from 0.5398 to 0.7945. This suggests that there is some effect of the type of airfoil. When n is allowed to vary, an improved fit is observed in both cases for an increase to n = 0.5997 and 0.6345 for all and NACA0012 profiles respectively This indicates a higher lift augmentation is observed at higher mini-tab heights than predicted by thin airfoil theory, consistent with the work of Greenwell[30].

In both figures, the mini-tab placed at x_f/c = 0.95 for the current study is indicated, with an increase in the change in lift observed for h/c = 0.04 than 0.02. It can be observed that the results generated in the current study lie close to both free and fixed n trends and within the range of results when both all airfoil profiles and NACA0012 profiles are considered. The agreement with literature is therefore excellent.

Comparing the present study to literature for locations away from the trailing edge is difficult, due to a scarcity in results and theoretical models. The closest survey is that of Baker et al[18] for a S809 airfoil, where the results for mini-tab placement at x_f/c = 0.40 compares extremely favourably to that of the current survey at x_f/c = 0.08. No lift reduction was observed before zero degrees, however the mini-tab's effectiveness towards stall increases. The difference in chord-wise location may also imply an effect due to the airfoil profile, however a more wide ranging study into this effect is required.

C. Particle Image Velocimetry Measurements

Fig. 7 and Fig. 8 present time-averaged velocity magnitude for both mini-tab heights (h/c = 0.02 & 0.04), alongside the baseline conditions without a mini-tab. PIV measurements were performed at five angles of attack (α = 0, 5, 8, 10 and 13°), and three locations (x_f/c = 0.08, 0.60 and 0.95). The C_L vs. α curves for the three locations and baseline configuration is presented above the PIV data with angles of interest highlighted by a vertical red line. When the angle of attack is increased, the baseline configuration illustrates the expected trend: the flow begins to separate from the trailing edge, with the separation point moving towards the leading edge consistent with trailing edge stall.

Fig. 7 shows time-averaged velocity magnitude data for mini-tabs of height, h/c = 0.02. Analysing the flow field close to the trailing edge (x_f/c = 0.95) allows for comparison to conventional Gurney flap utilization at zero degrees due to the symmetric profile used. At zero degrees a small separation region is observed behind the mini-tab. This separation region is formed of a counter-rotating vortex pair as theorized by Liebeck[6]. Reviewing the literature, placement close to the trailing edge indicates that the vortex pair produces a negative camber effect on the flow by shifting the Kutta condition away from the surface, reducing lift at low angles of incidence.

As the angle of attack approaches stall the natural separation point moves forward from the trailing edge. For both mini-tab heights a gradual reduction in lift mitigation is observed as the angle of attack is increased. At α = 13° the mini-tab of height h/c = 0.02 (Fig. 7) appears to be fully submerged within the natural separation region, while the force measurements display no change in lift for this configuration. In comparison, for a mini-tab of h/c = 0.04 effectiveness at the high angles of incidence is diminished but retained. At α = 13° this configuration still has some influence outside of the shear layer, allowing the mini-tab to still produce a small reduction in lift (ΔC_L = -0.15). The submersion within the recirculation region will also have an effect on drag, which can be observed in the force measurement in Fig. 4. As the mini-tab becomes engulfed in the separated flow region the drag increment diminishes.

Moving forward to x_f/c = 0.60 a more significant lift reduction is produced at low incidences when compared to x_f/c = 0.95 (ΔC_L = -0.60 vs -0.48 for h/c =0.04). The flow fields in Fig. 7 and Fig. 8 display a large separation region behind the tab for both heights, advancing separation in comparision to the baseline configuration at all angles of attack. This is reflected in the force measurements, where a significant but decreasing lift reduction is observed up to stall. Increasing mini-tab height has the effect of displacing the shear layer away from the surface creating a larger separation region behind the tab as shown in Fig. 8.

Placement at x_f/c = 0.08 produces a very different effect. At zero degrees a mini-tab of height, h/c = 0.02 induces a separation bubble which reattaches close to the mid-chord (Fig. 7), with flow accelerated outside of the shear layer. In comparision, Fig. 8 indicates that a mini-tab of height, h/c = 0.04 produces a separated region which extends beyond the trailing edge. However, corroboration with the force data indicates that even though the flow for this configuration is separated, neither configuration produces a significant reduction in lift (ΔC_L = -0.03 and -0.04 for h/c = 0.02 and 0.04 respectfully). Note that x_f/c = 0.08 also produced a large increment in drag coefficient at zero degrees increasing drag from C_D = 0.018 to 0.085 for a height, h/c = 0.04. The large flow separation induced by this case creates a significant increase in drag.

When compared to the baseline configuration, placement close to the leading edge appears to significantly advance the separation point even at stall. Increasing the angle of attack to 5° and beyond produces a more meaningful reduction in lift for both configurations, with h/c = 0.04 producing a more significant effect. The increase in lift reduction occurs in close agreement to the displacement of the shear layer and increase in separated region behind the mini-tab, indicating that this region is key to the lift mitigation of this configuration.

D. Pressure Measurements

In light of the PIV measurements, pressure measurements were performed for select cases. These cases are shown in Fig. 9 for an angle of attack of zero degrees. Fig. 9 shows C_P vs. x/c distributions for baseline, x_f/c = 0.08, 0.60 and 0.95 for h/c = 0.04 and x_f/c = 0.08 for h/c = 0.02 at zero degrees. Analysis of the baseline condition indicates that the pressure distribution at α = 0° was asymmetric with a lower suction peak and increased suction towards the trailing edge on the upper surface. The asymmetry may be due to a slight asymmetry induced in the NACA0012 profile by the presence of the slots, as described in section II.A. Zero lift was through an integration of the pressure measurements at zero degrees and is in good agreement with the previously described force measurements. The baseline pressure distribution is compared to an inviscid solution generated using Xfoil[31], with a good agreement shown in Figs. 9 to 11 for angles of attack of 0 to 8°.

Fig. 9(a) compares x_f/c = 0.95 to the baseline configuration. Placement close to the trailing edge has been previously evaluated in the literature and the results produced during the current study compare favourably. On the upper surface, a reduction in suction can be observed by the increase in C_P. In conjunction, an increase in suction can be observed on the lower surface, with peak suction increased from $C_{P,min}$ = -0.39 to -0.92. The same trend can be noted in the work of Cooperman et al[32]. The lack of pressure taps beyond x/c = 0.94 means that the pressure difference across the mini-tab and the pressure difference at the trailing edge could not be analysed fully, however the trends in the data presented suggests that a pressure difference is present at the trailing edge. This is supported by the work of Jeffrey et al[33] for a Gurney flap, whereby the final part of the pressure recovery is completed in the wake due to the displacement of the Kutta condition.

The placement of a mini-tab of height h/c = 0.04 at x_f/c = 0.60 (Fig. 9(b)) shows a similar increase in suction over the lower surface of the airfoil with a similar $C_{P,min}$. The placement of the mini-tab at this location appears to produce a large discontinuity in the pressure distribution, with increasing C_P ahead of the mini-tab when compared to the baseline condition. A pair of missing pressure taps at x/c = 0.57 and 0.62 mean that the pressure difference directly across the mini-tab could not be fully evaluated. Behind the mini-tab the flow is separated from the airfoil surface reflected in the measurements by the region of constant $C_P \approx$ -0.5.

In the description of the PIV measurements for placement close to the leading edge (x_f/c = 0.08) a difference in the flow structure between h/c = 0.02 and 0.04 was noted, however no noticable difference in C_L was observed. Further investigation using pressure measurements is presented in Figs. 9(c) and (d). For both mini-tab cases an increase in C_P towards 1 can be observed, suggesting a stagnation in the flow ahead of the mini-tab. On the lower surface, once again an increase in suction is noted, with a lower severity for h/c = 0.02 than 0.04.

Behind the mini-tab the trends for the two heights differ greatly. For h/c = 0.02 the separation bubble can be clearly observed. The trend in pressure coefficient observed in the mini-tab induced separation bubble is in close agreement with those for natural laminar separation bubbles characterized by Horton[34] who indicated that the initial, laminar flow region is charactized by a region of near constant velocity and hence pressure. Transition to turbulence is indicated by a decrease in velocity and a corresponding increase in C_P. Observing the data presented in Fig. 9(d) and comparing it to the trends described, a transition to turbulent flow can be observed at $x/c \approx$ 0.27 with an increase in C_P and

reattachment at $x/c \approx 0.47$. Beyond reattachment, the pressure distribution matches closely to that for the baseline configuration. For $h/c = 0.04$ (Fig. 4(c)), a lower suction peak can be observed ($C_{P,min}$ = -0.45 vs. -0.7). A turbulent transition point is suggested at $x/c \approx 0.5$ however reattachment does not occur with a difference in C_P observable to the trailing edge. In both cases, it appears that the increase in suction caused by the acceleration of flow on the lower surface is balanced by the stagnation ahead and separation of flow behind the mini-tab on the upper surface, thus producing no significant difference in C_L.

Figs. 10 and 11 present surface pressure distributions for five and eight degrees. For the baseline configuration a good agreement to the inviscid Xfoil solution is observed, with similar peak suction, $C_{P,min}$ and adverse pressure gradient. Comparing Figs. 10(a) and 11(a) a trend for placement in the vicinity of the trailing edge can be noted. Ahead of the mini-tab located at $x_f/c = 0.95$, an increase in pressure over the upper surface can be observed in comparison to the baseline configuration, reducing lift. At 5°, the finite pressure difference at the trailing edge is retained, however at 8° it is much less prominent. In conjunction, the difference in pressure over the upper surface is reduced. In comparison to both 5° and 0° a reduction in change in lift, ΔC_L. Concurrent analysis with Fig. 6 indicates that a region of separated flow is present ahead of the $h/c = 0.04$ mini-tab at $x_f/c = 0.95$ suggesting that the flow separation causes a reduction in influence on the flow for this location as α increases. For a close to trailing edge configuration the finite pressure difference at the trailing edge is key to effective lift reduction, causing the final part of pressure recovery to be completed in the wake and reducing suction over the upper airfoil surface.

Figs. 10(b) and 11(b) illustrate the pressure distribution at $x_f/c = 0.60$ for 5° and 8°. In comparison to baseline, the magnitude of C_P is greatly reduced producing lower lift. Constant C_P behind the mini-tab indicates separated flow, confirmed by the PIV measurements (Fig. 7). The difference in pressure across the mini-tab is retained between 0° and 5°, however a reduction is noted at 8° consistent with a reduction in ΔC_L. Once again, as the natural flow separation propagates upstream the pressure difference across the mini-tab decreases, reducing effectiveness in lift mitigation.

For placement towards the leading edge at $x_f/c = 0.08$ an opposing trend in ΔC_L was observed near stall when compared to trailing edge placement. Pressure coefficient measurements presented in Figs. 10 and 11(c) indicate that the region of stagnation ahead of the mini-tab is retained as α is increased. Behind the mini-tab, constant C_P of -0.4 indicates an intensification of the separation region in comparison to $\alpha = 0°$ and is prevalent at both 5° and 8°. The separated flow over the majority of the upper surface greatly reduces the lift produced, generating a large ΔC_L. As α is increased the suction peak is effectively eliminated by mini-tab placement at $x_f/c = 0.08$. Using Fig. 7 an increase in C_L is observed between 5° and 8° from 0.14 to 0.23. The C_P distributions indicate that between 5 and 8° a significant change in pressure is only observed on the lower surface of the airfoil, where an increase in positive pressure increases the overall lift produced.

E. Unsteady Force and Instantaneous Flow Fields

In order to investigate the unsteady fluctuations in force produced by mini-tab employment the standard deviation of lift coefficient (σ_{CL}) is displayed in Fig. 12. In conjunction, a series of instantaneous flow field measurements are displayed in Figs. 13 and 14 to illustrate the mini-tab's effect. The baseline configuration illustrates an increase in unsteadiness close to stall, consistent with the large, unsteady flow behavior produced at this condition.

For both heights, with $x_f/c = 0.95$ σ_{CL} is increased in comparison to the baseline for low angles of incidence, with a larger standard deviation in C_L observed for $h/c = 0.04$ when compared to $h/c = 0.02$ (σ_{CL} = 0.018 and 0.011 respectively). Instantaneous flow-field measurements displayed in Fig. 13(a) indicates that behind the mini-tab at $x_f/c = 0.95$ an unsteadiness exists within the wake region, indicating the formation of a von Karman vortex street behind the mini-tab. This is consistent with the observations of Neuhart & Pendergraft[35] for the conventional Gurney flap. As α approaches stall, the difference in σ_{CL} diminishes towards the baseline configuration. The decrease is consistent with the time-averaged C_L information presented, thus the return to baseline σ_{CL} is as expected. Analysing Figs. 14 (a) and (b) the instantaneous flow-field at both 5° and 8° suggests that some flow separation is exhibited ahead of the mini-tab, reducing the influence on the flow consistent with a decrease in lift reduction. At these angles the vortex shedding from the mini-tab becomes less prominent, reducing σ_{CL} towards the baseline condition.

For $x_f/c = 0.60$ a similar trend is observed with increase in unsteadiness for the greater mini-tab height. In Fig. 12, the standard deviation in C_L decreases with increasing angle of attack, returning to the baseline trend at 4° and 6° for heights of $h/c = 0.02$ and 0.04 respectfully. Analysis of the instantaneous flow-field from Figs. 13(b) and (c) indicates that the unsteady flow separation behind the mini-tab of $h/c = 0.04$ is enlarged compared to the $h/c = 0.02$ mini-tab, increasing the standard deviation in C_L. At 5° and 8° (Figs. 14(c) to (f)) the unsteady shear layer is displaced away from the airfoil surface, with some separation observed ahead of the mini-tab location. The unsteadiness away from the surface of the aerofoil has a reducing influence, thus σ_{CL} is reduced.

When the mini-tab is located in the vicinity of the leading edge, it was found that σ_{CL} was extremely dependent on the mini-tab height. For h/c = 0.02 no change was observed at 0°, whereas a large increase was observed for h/c = 0.04 (σ_{CL} = 0.028). Analysis of the instantaneous flow-field in Figs. 13 (d) and (e) indicates that a larger unsteady flow separation is present for h/c = 0.04 than 0.02. The small scale flow-structures present in Fig. 13 (d) indicate a small effect on the unsteadiness in C_L. Fig. 13 (e) illustrates an increased wake width behind the mini-tab for h/c = 0.04, with an increased curvature in the streamlines suggesting increased unsteadiness in the wake region, producing an increase in σ_{CL}. At 5°, it was found that h/c = 0.02 produced a large increase in σ_{CL} to a value of 0.047, whereas h/c = 0.04 produced a lower value of 0.033. Fig. 14(g) indicates that the shear layer for h/c = 0.02 is close to the surface of the airfoil and provides only a partial detachment of the flow at certain instances. This behavior is masked by the time-averaging process. In comparison, h/c = 0.04 (Fig. 14(h)) produces a shear layer which fully detaches flow over the upper surface of the airfoil. It is theorized that the unsteady detachment and reattachment of the flow from the upper surface increases the unsteady forces observed by the airfoil profile at both 5° and 8°. For h/c = 0.04 the phenomena is not observed, thus a reduction in σ_{CL} is noted when compared to h/c = 0.02.

IV. Conclusions

Force, particle image velocimetry and pressure measurements are presented for mini-tabs of various heights and chord-wise locations. It is shown that lift mitigation increased with mini-tab height at all chord-wise locations, however the effect of chord-wise position is dependent on the angle of attack. Close to the trailing edge, the mini-tab is found to produce a large lift reduction at low angles of incidence, displacing the Kutta condition into the wake and producing an increased pressure difference consistent with literature. At higher angles, the mini-tab becomes immersed within the natural separation region, decreasing effectiveness. Placement at x_f/c = 0.60 is found to produce a constant ΔC_L at low incidences, suggesting it may be an ideal location for aircraft at cruise with a decrease in effectiveness at high angles of attack as the mini-tab once again became immersed in the natural separation region. Conversely, placement close to the leading edge (x_f/c = 0.08) induces a negligible effect at zero degrees, despite the presence of a large separation region behind the mini-tab. The mini-tab displaces the shear layer further away from the airfoil surface and appears to be the key to increased lift reduction at higher angles of attack. Analysis of the unsteady force and instantaneous flow field indicated an increase in the standard deviation in lift coefficient for x_f/c = 0.08 and h/c = 0.02, where an unsteady detachment and reattachment of flow from the upper surface of the airfoil was observed.

Acknowledgments

The authors would like to thank Airbus UK for the financial support supplied to this project. The author's work was supported by a University Research Studentship by the University of Bath.

References

[1]Andersen, P. B.. "Advanced Load Alleviation for Wind Turbines Using Adaptive Trailing Edge Flaps: Sensoring and Control.", *Ph.D. Thesis*, Technical University of Denmark, 2010.

[2]J. Heinz, N.N. Sorensen, and F. Zahle. "Investigation of the load reduction potential of two trailing edge flap controls using CFD", *Wind Energy*, Vol 14, 2011, pp.449-462

[3]Kral, L.D., "Active flow control technology", *ASME Fluids Engineering Division Newsletter*, 1999: pp. 3-6.

[4]Gad-el-Hak, M., "Flow Control: The Future", *Journal of Aircraft*, Vol. 38, No. 3, 2001, pp 402-418.

[5]Johnson, S. J., Baker, J. P., Van Dam, C. P., Berg, D, "An overview of active load control techniques for wind turbines with an emphasis on microtabs", *Wind Energy*, Vol. 13, No. 2-3, 2010, pp. 239-253.

[6]Liebeck, R.H., "Design of Subsonic Airfoils for High Lift", *Journal of Aircraft*, Vol. 15, No. 9, 1978, pp. 547-561.

[7]Gai, S.L. and Palfrey, R. "Influence of Trailing-Edge Flow Control on Airfoil Performance", *Journal of Aircraft*, Vol. 40, No. 2, 2003, pp. 332-337.

[8]Myose, R., Papadakis, M. and Heron, I., "Gurney flap experiments on airfoils, wings, and reflection plane model" *Journal of Aircraft*, Vol. 35, 1998, pp. 206-211.

[9]Van Dam, C.P., Yen, D.T., and Vijgen, P.M. H. W., "Gurney Flap Experiments on Airfoil and Wings". *Journal of Aircraft*, Vol. 36, No. 2 , pp. 484-486.

[10]Date, J.C. and Turnock, S.R., "Computational evaluation of the periodic performance of a NACA 0012 fitted with a Gurney flap", *Journal of Fluids Engineering*, Vol. 124, No. 1, 2002**,** pp. 227-234.

[11]Liu, T. and Montefort, J., "Thin-Airfoil Theoretical Interpretation for Gurney Flap Lift Enhancement", *Journal of Aircraft*, Vol. 44, No. 2, 2007, pp. 667-671.

[12]Brown, L. and Fillipone, A., "Airfoil at low speeds with Gurney flaps", *Aeronautical Journal*, Vol. 107, No. 1075, 2003, pp. 539-546.

[13]Matalanis, C. G., Wake, B. E., Opoku, D., Min, B-Y., Yeshala, N. and Sankar, L., "Aerodynamic Evaluation of Miniature Trailing-Edge Effectors for Active Rotor Control", *Journal of Aircraft*, Vol. 48, No. 3, 2011, pp. 995-1004.

[14] Cooperman, A.M., Chow, R. and van Dam, C.P., "Active Load Control of a Wind Turbine Airfoil Using Microtabs", *Journal of Aircraft*, 2013. Vol 50., No. 4, 2013, pp. 1150-1158.

[15] Nakafuji, D.Y., Van Dam, C. P., Smith, R. L. and Collins, S. D., "Active load control for airfoils using microtabs", *Journal of Solar Energy Engineering*, Vol. 123, No. 4, 2001, pp. 282-289.

[16]Wang, J., Li, Y. and Choi, K.-S., "Gurney flap—Lift enhancement, mechanisms and applications*"*, *Progress in Aerospace Sciences*, Vol. 44, No. 1, 2008, pp. 22-47.

[17]Li, Y., Wang, J. and Zhang, P., "Influences of Mounting Angles and Locations on the Effects of Gurney Flaps". *Journal of Aircraft*, Vol. 40, No. 3, 2003, pp. 494-498.

[18] Baker, J.P., Standish, K. J. and Van Dam, C. P., "Two-dimensional wind tunnel and computational investigation of a microtab modified airfoil", *Journal of Aircraft*, Vol. 44, No. 2, 2007. pp. 563-572.

[19] Pankhurst, R. C. and Holder, D. W., *Wind Tunnel Technique: An Account of Experimental Methods in Low- and High- Speed Wind Tunnels*, 1st Edition, Pitman, London, pp. 462- 465.

[20] Barlow, J. B., Rae, J. B., and Pope. A., *Low-speed wind tunnel testing*, John Wiley & Sons., 1999, pp. 309.

[21]Cleaver, D .J., Wang, Z., Gursul, I. and Visbal, M. R., "Lift Enhancement by Means of Small-Amplitude Airfoil Oscillations at Low Reynolds Numbers", *AIAA Journal*, Vol. 49, No. 9., 2011, pp. 2018-2033.

[22]Gursul, I., Cleaver, D. J., and Wang, Z., "Control of low Reynolds number flows by means of fluid–structure interactions". *Progress in Aerospace Sciences*, Vol. 64, 2014, pp. 17-55.

[23]Moffat, R.J., "Describing the uncertainties in experimental results", *Experimental Thermal and Fluid Science*, Vol. 1, No. 1, 1988, pp. 3-17.

[24]Jacobs, E. N., and Sherman, A. "Airfoil section characteristics as affected by variations of the Reynolds number", National Advisory Committee for Aeronautics , 1937.

[25]Sheldahl, R.E. and Klimas, P. C., "Aerodynamic characteristics of seven symmetrical airfoil sections through 180-degree angle of attack for use in aerodynamic analysis of vertical axis wind turbines". 1981, Sandia National Labs., Albuquerque.

[26] Gault, D. E., "A correlation of low-speed, airfoil-section stalling characteristics with Reynolds number and airfoil geometry", National Advisory Committee for Aeronautics, 1957.

[27] Li, Y., Wang, J. and Zhang, P., "Effect of Gurney Flaps on a NACA0012 Airfoil", *Journal of Flow, Turbulence and Combustion*, Vol. 68, No. 1, 2002, pp. 27-39

[28] Storms B.L. and Jang, C.S., "Lift Enhancement of an Airfoil Using a Gurney Flap and Vortex Generators", *Journal of Aircraft*, Vol 45, No. 6, 1994, pp. 542-547

[29] Maughmer, M.D. and Bramesfeld, G., "Experimental Investigation of Gurney Flaps", *Journal of Aircraft*, Vol 45, No. 6, 2008, pp. 2062- 2067

[30] Greenwell, D.I., "Gurney Flaps on Slender and Nonslender Delta Wings", *Journal of Aircraft*, Vol 47, No. 2, 2010, pp. 675- 681

[31]Drela, M. "XFOIL: An analysis and design system for low Reynolds number airfoils." *Low Reynolds number aerodynamics*. Springer Berlin Heidelberg, 1989, pp. 1-12.

[32]Cooperman, A.M., "Wind tunnel testing of microtabs and microjets for active load control of wind turbine blades", PhD Thesis, University of California, Davis, 2013.

[33]Jeffrey, D., X. Zhang, and D.W. Hurst, "Aerodynamics of Gurney Flaps on a Single-Element High-Lift Wing", *Journal of Aircraft*, Vol. 37, No. 2, 2000, pp. 295-301.

[34]Horton, H. P., "A semi-empirical theory for the growth and bursting of laminar separation bubbles", HM Stationery Office, 1969.

[35]Neuhart, D.H. and Pendergraft O.C.,"Water Tunnel Study of Gurney Flaps", NASA TM4071, November 1988

Figures

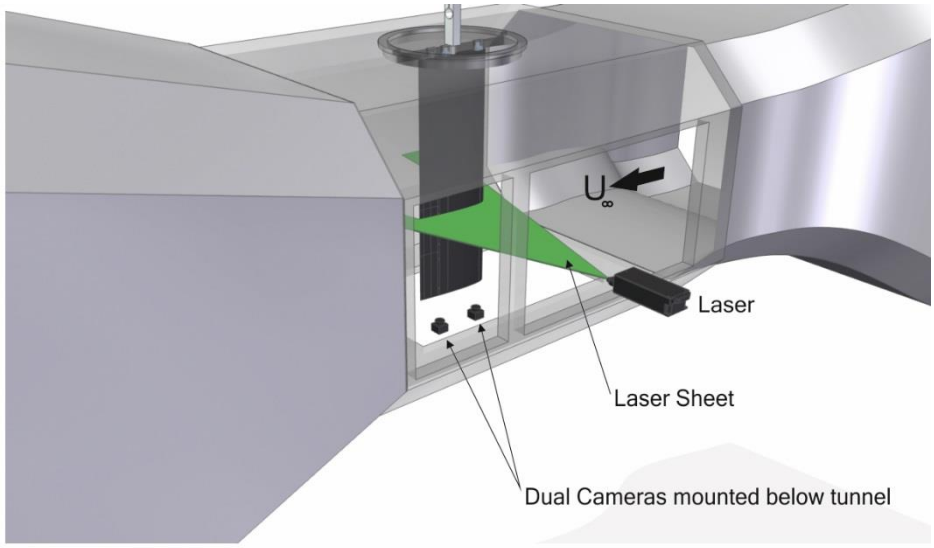

a)

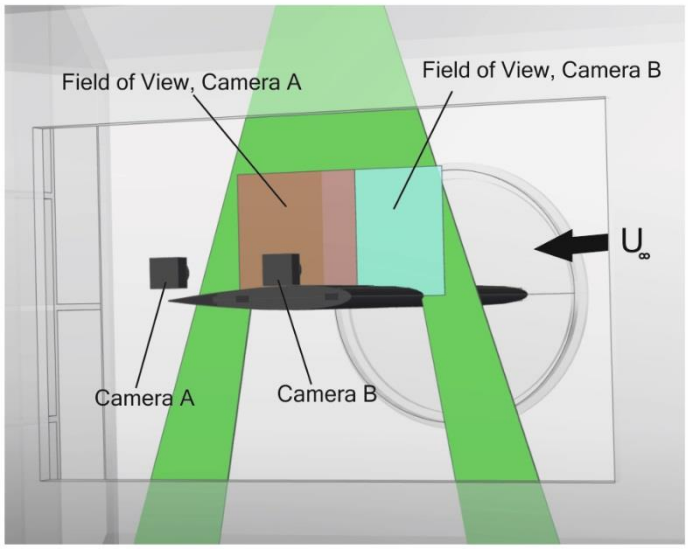

b)

Figure 1: Experimental Set-up for Particle Image Velocimetry measurement shown (a) from the side and (b) from below highlighting the fields of view of the tandem cameras.

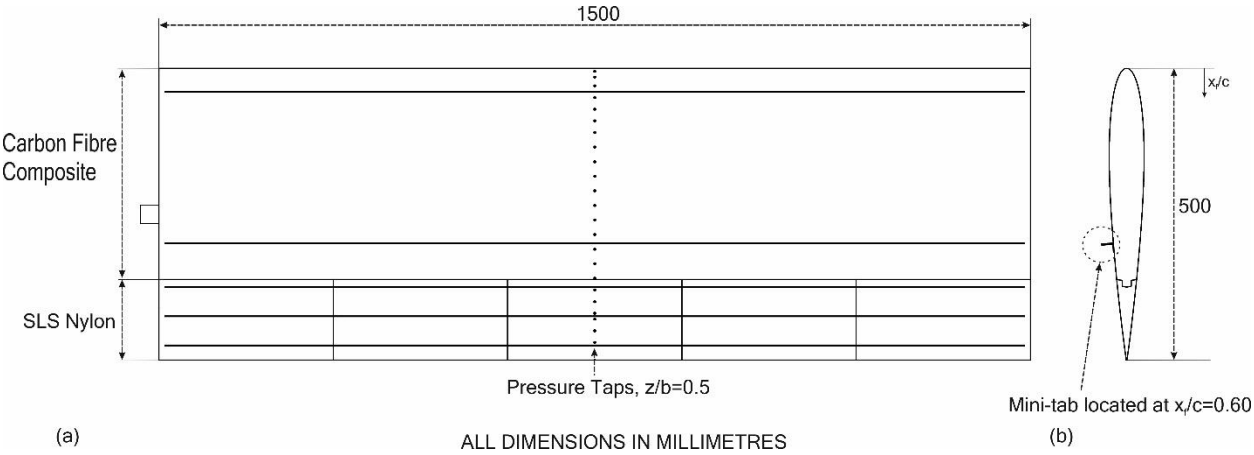

Figure 2: (a) Span-wise view of the wing, (b) Chord-wise illustration of the airfoil displaying an example of mini-tab of height, h/c = 0.04.

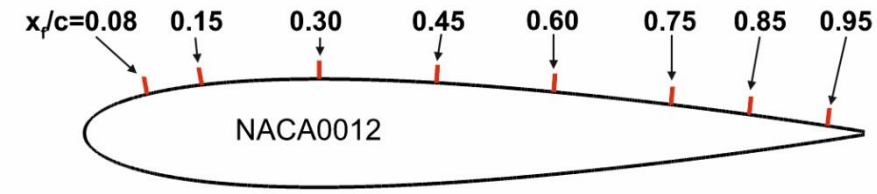

Figure 3: Schematic of NACA0012 profile, illustrating the mini-tab locations.

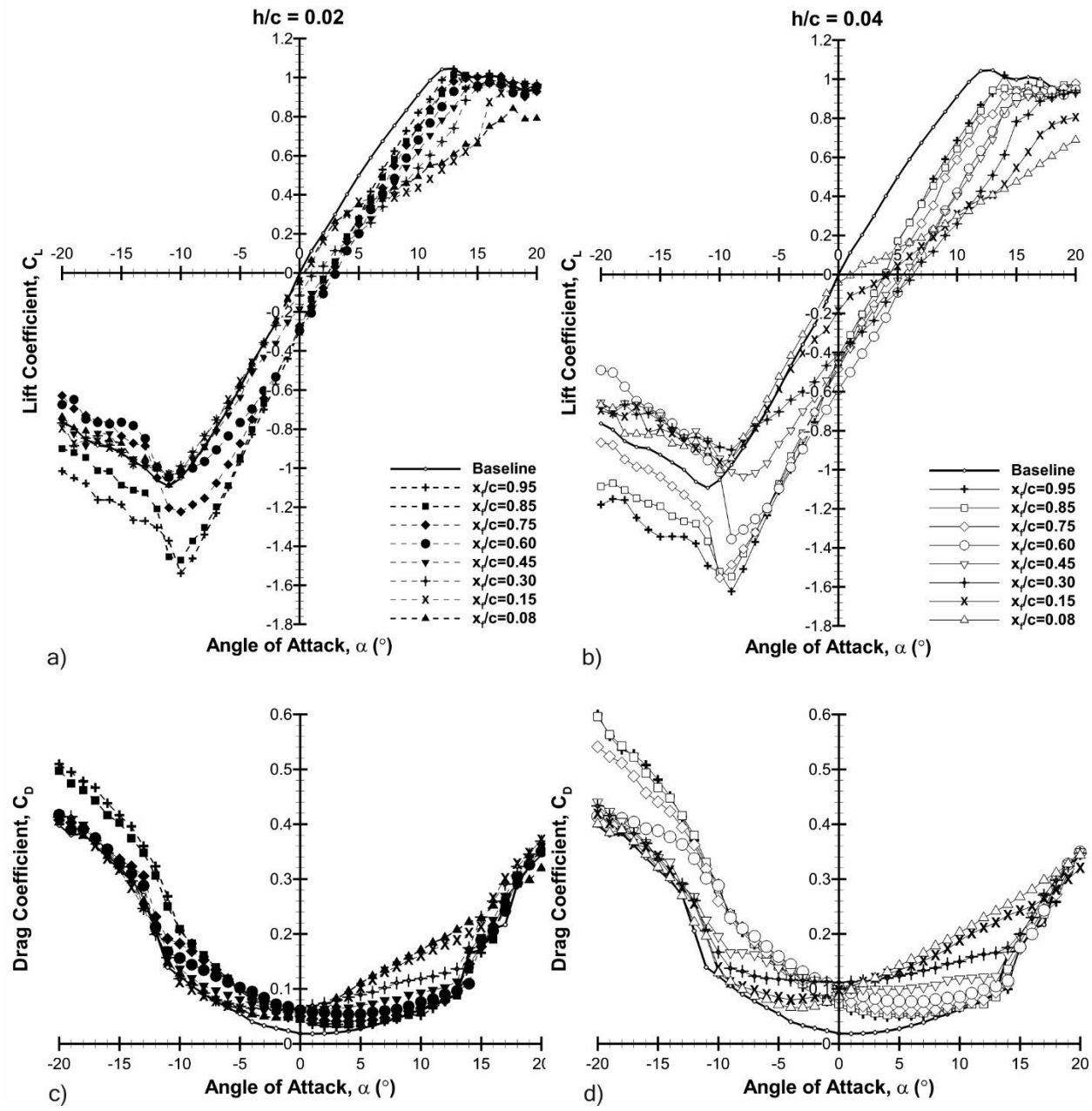

Figure 4: Time-averaged lift and drag coefficients vs. angle of attack for heights, h/c=0.02 (a & c) & 0.04 (b & d) and varying chord-wise location.

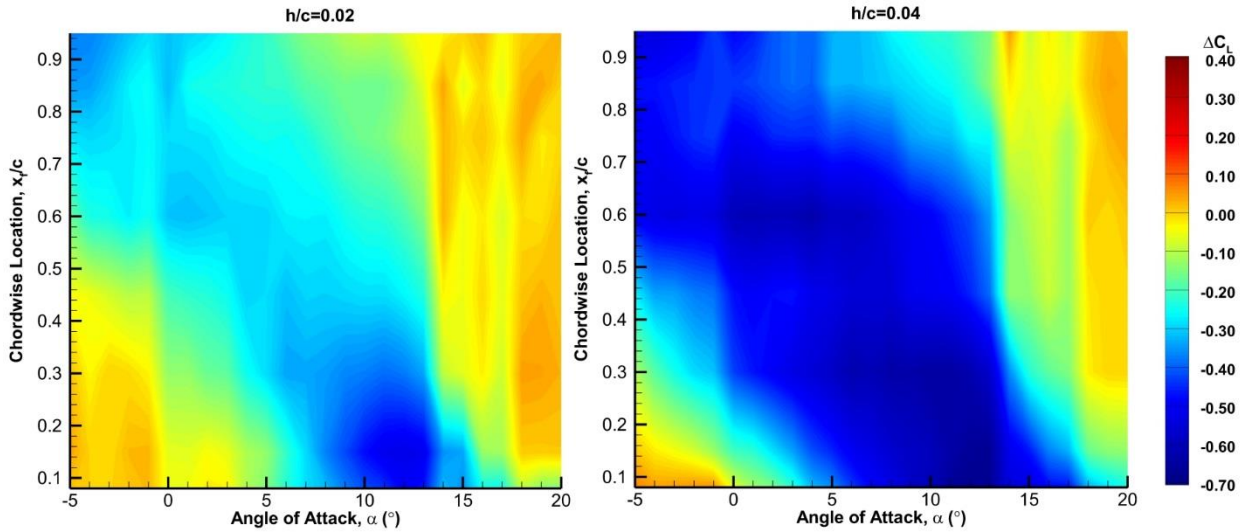

Figure 5: Contours of change in time-averaged lift coefficient (ΔC_L) as a function of chord-wise location and angle of attack for mini-tabs of height (a) h/c = 0.02 & (b) 0.04.

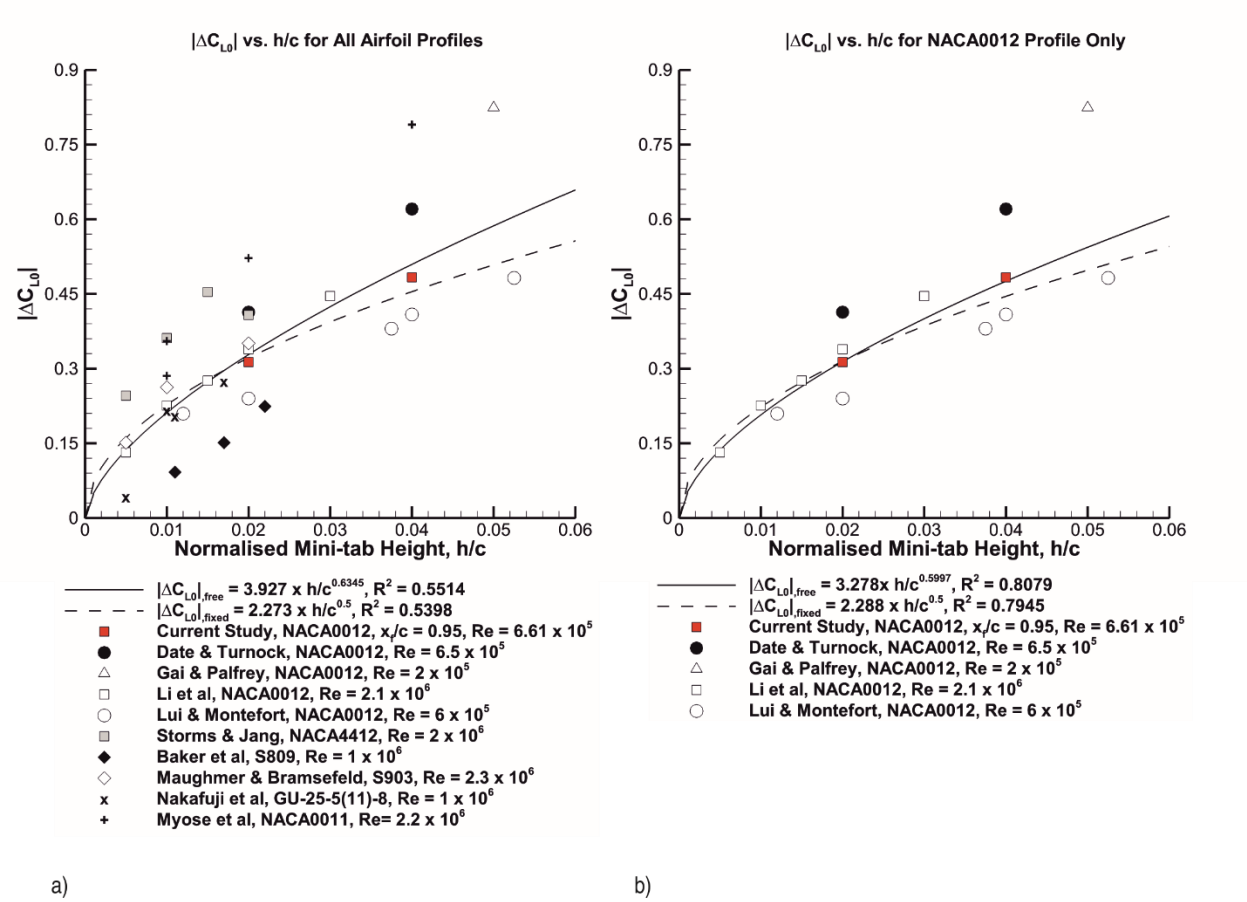

Figure 6: Magnitude of change in lift at zero lift angle ($|\Delta C_{L0}|$) as a function of mini-tab height for (a) all airfoil profiles and (b) NACA0012 profiles only. Trend lines illustrate Liu and Montefort[11] method with and without a variable exponent, n.

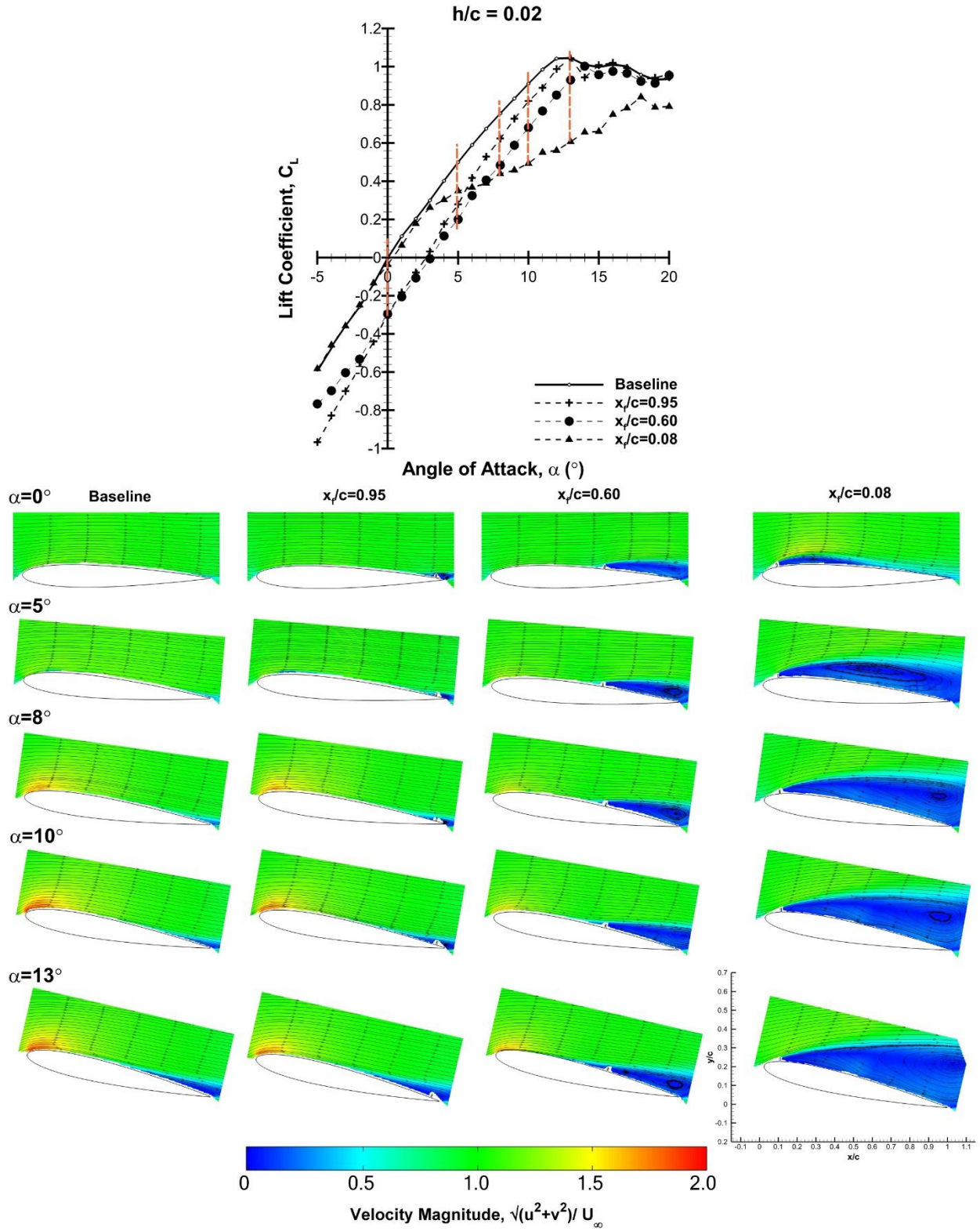

Figure 7: Lift coefficient vs. angle of attack for h/c=0.02. Corresponding normalized velocity magnitude shown for three example chord-wise locations at the angles of attack indicated by the red vertical lines in the lift coefficient plot.

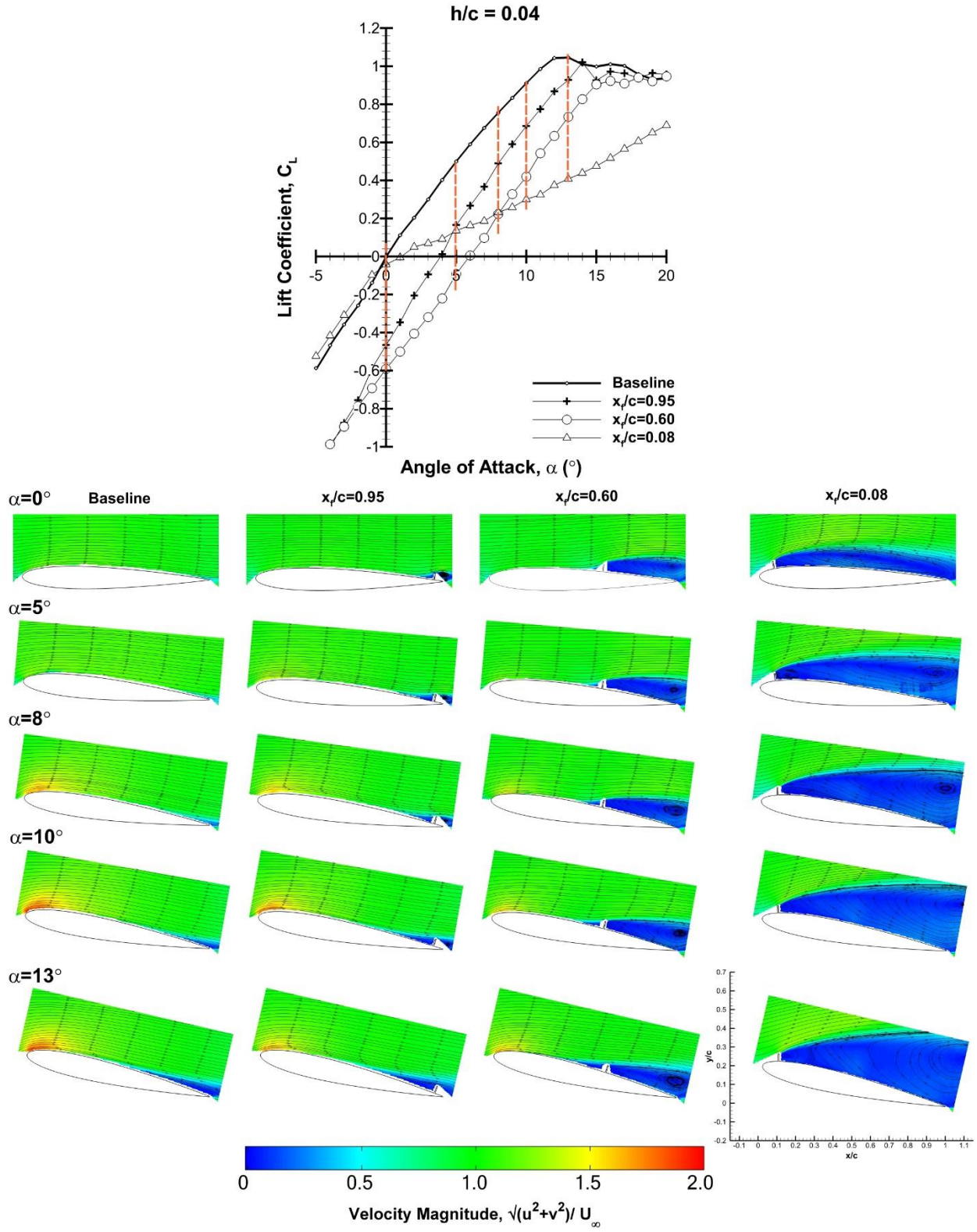

Figure 8: Lift coefficient vs. angle of attack for h/c=0.04. Corresponding normalized velocity magnitude shown for three example chord-wise locations at the angles of attack indicated by the red vertical lines in the lift coefficient plot.

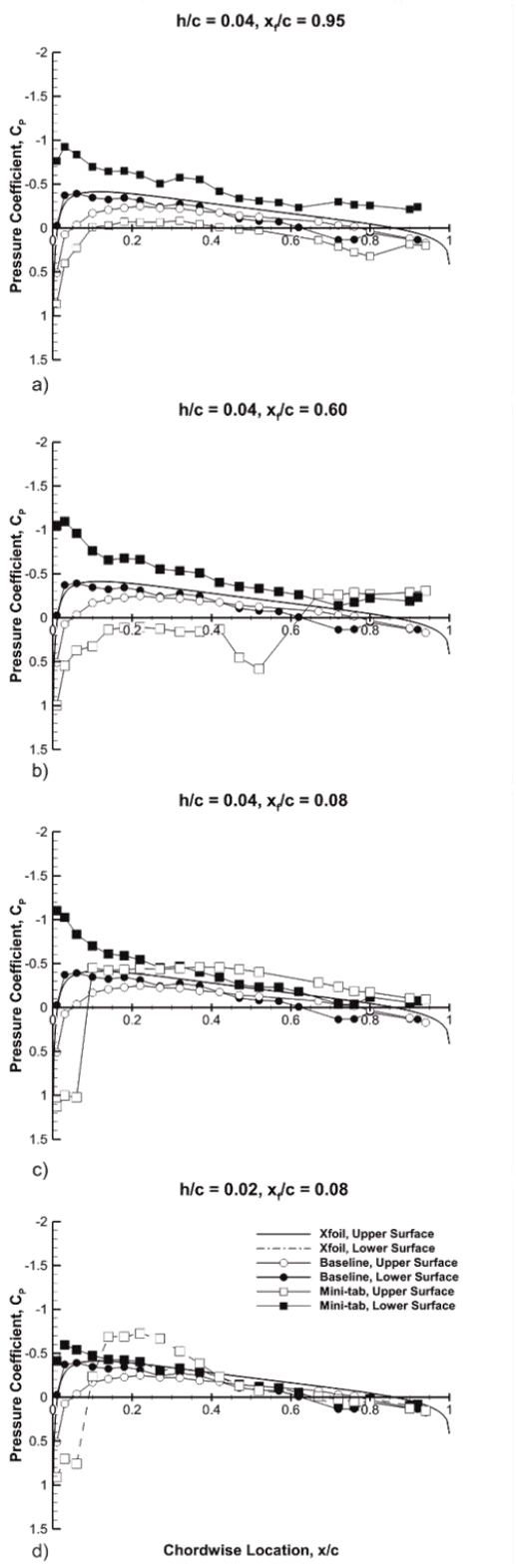

Figure 9: Pressure coefficient (C_P) vs. chord-wise location (x/c) at an angle of attack of zero degrees for (a) h/c = 0.04, x_f/c = 0.95, (b) h/c = 0.04, x_f/c = 0.60, (c) h/c = 0.04, x_f/c = 0.08, (d) h/c = 0.02, x_f/c= 0.08. Comparison to baseline and inviscid solution generated by XFOIL also presented for α = 0°.

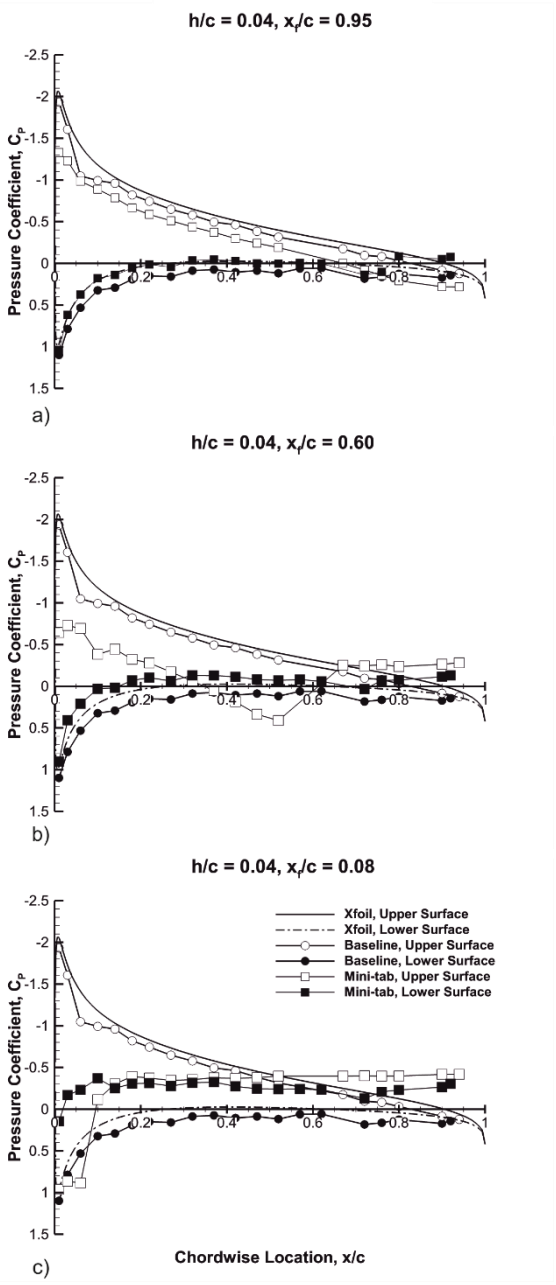

Figure 10: Pressure coefficient (C_P) vs. chord-wise location (x/c) at an angle of attack of five degrees for (a) h/c = 0.04, x_f/c = 0.95, (b) h/c = 0.04, x_f/c = 0.60, (c) h/c = 0.04, x_f/c = 0.08. Comparison to baseline and inviscid solution generated by XFOIL also presented for α = 5°.

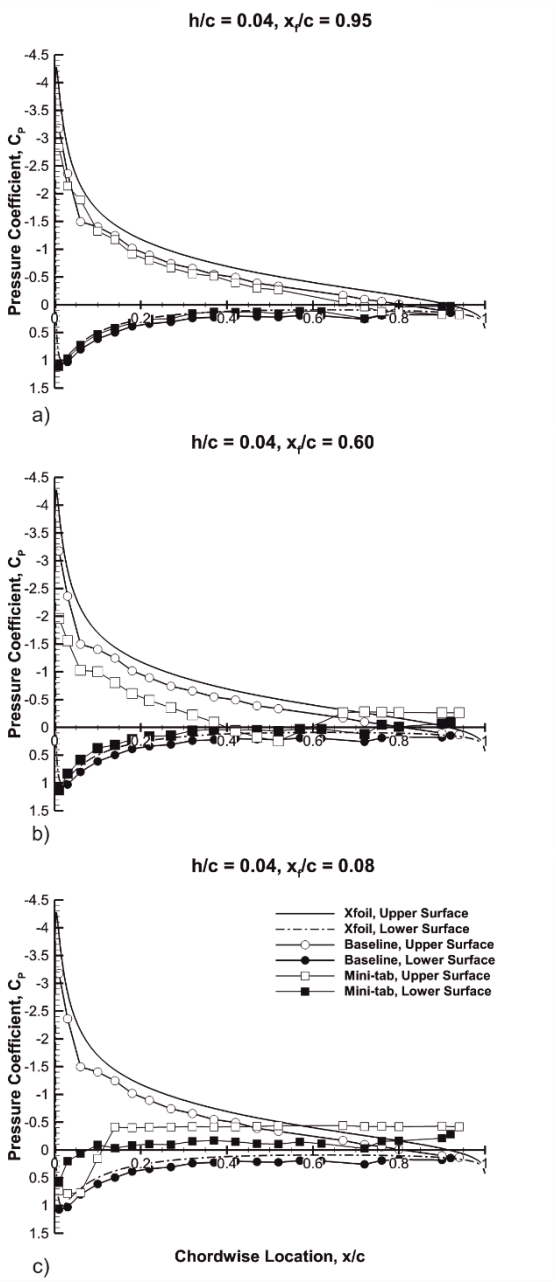

Figure 11: Pressure coefficient (C_P) vs. chord-wise location (x/c) at an angle of attack of eight degrees for (a) h/c = 0.04, x_f/c = 0.95, (b) h/c = 0.04, x_f/c = 0.60, (c) h/c = 0.04, x_f/c = 0.08. Comparison to baseline and inviscid solution generated by XFOIL also presented for α = 8°.

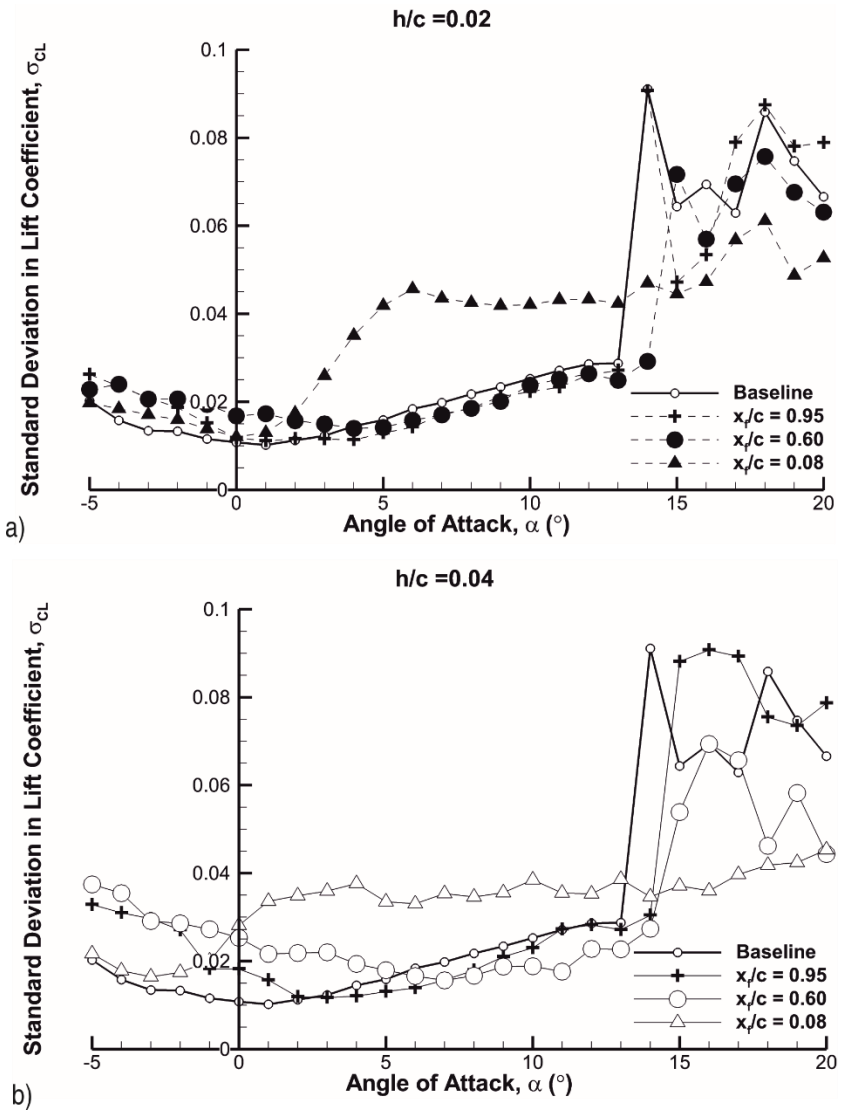

Figure 12: Standard deviation in lift coefficient (σ_{CL}) for mini-tab heights of (a) h/c = 0.02 & (b) h/c = 0.04

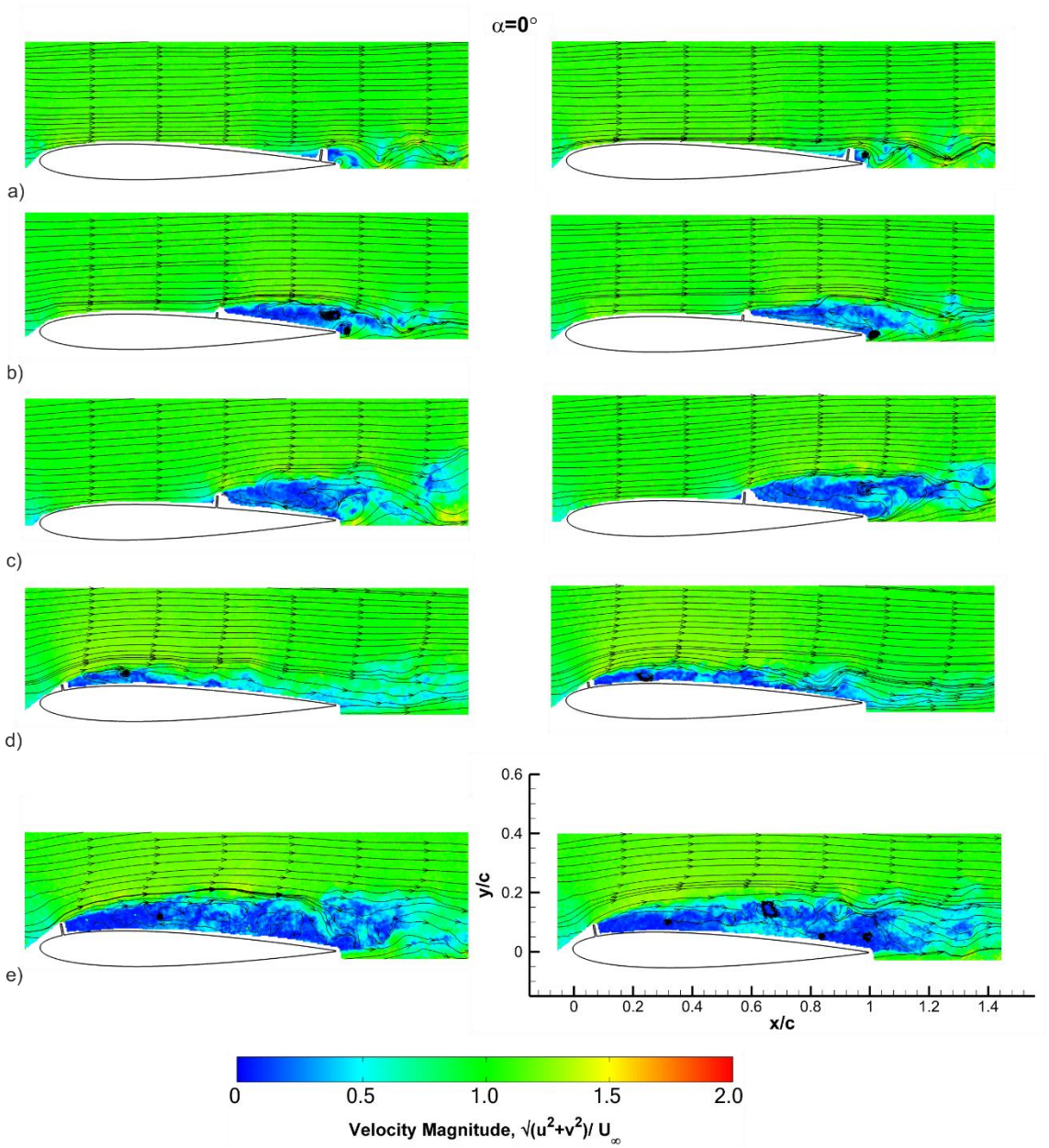

Figure 13: Instantaneous normalized velocity magnitude at zero degrees incidence presented for (a) x_f/c =0.95, h/c = 0.04, (b) x_f/c =0.60, h/c = 0.02, (c) x_f/c =0.60, h/c = 0.04, (d) x_f/c =0.08, h/c = 0.02, (e) x_f/c =0.08, h/c = 0.04.

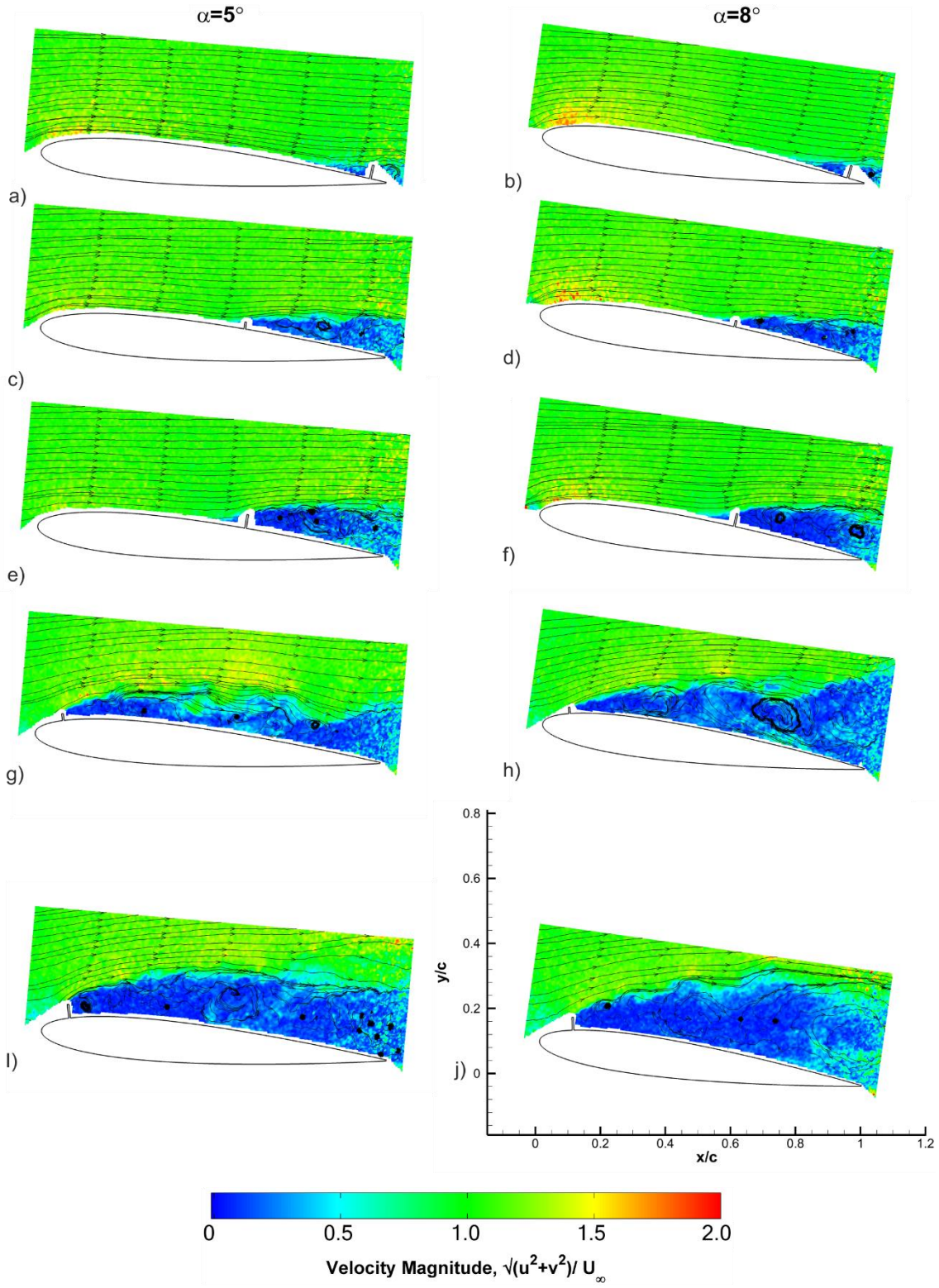

Figure 14: Instantaneous normalized velocity magnitude at five and eight degrees incidence presented for (a) and (b) x_f/c =0.95, h/c = 0.04, (c) and (d) x_f/c =0.60, h/c = 0.02, (e) and (f) x_f/c =0.60, h/c = 0.04, (g) and (h) x_f/c =0.08, h/c = 0.02, (i) and (j) x_f/c =0.08, h/c = 0.04.